IEEE Access
Multidisciplinary | Rapid Review | Open Access Journal

Received August 6, 2018, accepted October 24, 2018, date of publication November 12, 2018,
date of current version December 18, 2018.

Digital Object Identifier 10.1109/ACCESS.2018.2880741

Data Amount Reduction in Mosaic Image Transmission Techniques for Digital Interactive Television Applications

FREDDY R. ACOSTA-BUENAÑO[1,2], (Member, IEEE), INMACULADA MORA-JIMÉNEZ[2], GONZALO OLMEDO[1], (Member, IEEE), AND JOSÉ LUIS ROJO-ÁLVAREZ[2,3], (Senior Member, IEEE)

[1]Departamento de Eléctrica y Electrónica, Universidad de las Fuerzas Armadas ESPE, Sangolquí 170501, Ecuador
[2]Department of Signal Theory and Communications, Telematics and Computing Systems, Rey Juan Carlos University, 28943 Madrid, Spain
[3]Center for Computational Simulation, Universidad Politécnica de Madrid, 28223 Madrid, Spain

Corresponding author: Freddy R. Acosta-Buenaño (fracosta@espe.edu.ec)

This work was supported in part by the Research Projects Platform for Usability Analysis for Interactive Digital Television Applications under Grant 2013-PIT-016, in part by the Energy Efficiency in Wireless Sensor Networks from the Universidad de las Fuerzas Armadas ESPE, in part by the Spanish Government through the research KLINILYCS and FINALE under Grant TEC2016-75361-R and Grant TEC2016-75161-C2-1-R, respectively, and in part by PRICAM under Grant S2013/ICE-2933 from the Comunidad de Madrid.

ABSTRACT Several images are used as a part of the interactive data in the Nipo-Brazilian digital TV system that require good subjective quality while using the lowest possible bandwidth but the well-known traditional compression systems are already applied by default to these images. The concept of a mosaic image (several images forming one) has been formerly used in the steganography application field. The mosaic image is obtained by reordering the image-blocks of a secret image disguised as another image, the so-called target image, and then feeding both to a near reversible color-transformation algorithm. Its use is a possible solution to this need in digital interactive television, for which the main challenge is to achieve this by using less bandwidth for transmission. We propose here a procedure to reduce the amount of data needed to recover the secret image from the mosaic image, as well as a criterion to select the target image and therefore improve the quality of the recovered secret image in interactive data applications. The main objective is to efficiently transmit two images as one using a lower bandwidth. On the one hand, the number of bits needed to recover a given secret image is highly reduced by modeling the image-block standard deviation statistical distribution. On the other hand, the entropy of the image-block means and standard deviations per color component are used to identify the most convenient target image among the images set present in the interactive application of interest. A series of experiments with a set of 20 mostly natural images showed a reduction in the number of bits close to 3-to-1 with respect to techniques of reference. The proposed method allows us to improve the bandwidth use by reducing the number of bits needed to recover the secret image, it preserves the subjective quality of recovered secret images, and it gives the possibility to determine the best target images available in several multimedia and digital terrestrial television applications.

INDEX TERMS Digital terrestrial television, interactive applications, mosaic image, image entropy, image selection, nearly reversible color transformations.

I. INTRODUCTION

Digital Terrestrial Television (DTT) systems are implemented in almost all the world. In Ecuador and most of Latin America, part of Asia, and Africa, the Nipo-Brazilian Digital TV System (SBTVD, short for Sistema Brasileiro de Televisão Digital, also known as ISDB-Tb) has been defined. In ISDB-Tb, middleware GINGA is established as an intermediate software layer that allows the development of interactive applications for DTT. GINGA is also an ITU-T recommendation for Internet Protocol Television (IPTV) Services [1], and it also allows to use MPEG and AVI video, as well as JPEG, PNG and GIF images [2]. The data carousel of DTT has limited bandwidth for the transmission of multimedia related to interactive applications, hence, it becomes necessary to use it efficiently, in order to provide enough quality on the presentation of interactive applications.

Since images are the most commonly used multimedia elements in an interactive television application [3], a form to transmit the image set of any interactive application with the best bandwidth performance is still needed.

For this purpose, we propose to look for a method to transmit various images at a time, and in this setting, image blending techniques have been proposed for their use in Earth Sciences, which allow us to overlay relevant information from multiple images over a single one and view them in a single image [4]. Also, in the traditional information security system setting, the process of hiding information has been widely studied, and it has been stated as embedding secret data into different carriers of digital media, such as image, audio, or video streams [5]–[10]. On the other hand, many interactive applications work with image sets that could be naturally used as carriers. A new type of computer art image, called secret fragment-visible mosaic image, has been proposed [11] and used in other types of applications. In this precedent work, the mosaic image is automatically created by composing small fragments (image-blocks) of a given image (secret) to become a target image in a mosaic form, in which the target image is preselected from a working database. An improvement to the previously cited procedure has been proposed to avoid the large database requirement [12] by using the Nearly-Reversible Color Transformation (NRCT) method proposed in [13]. NRCT was used to match the color image-block statistics of a secret image with those of a target image, and it was able to work with any arbitrarily selected target image.

Furthermore, a new algorithm also based on [12] was presented in [14], in which the recovered secret image quality was numerically quantified. For this purpose, the color image-blocks were first characterized by their mean vectors and covariance matrices, and the mosaic image then was created by taking advantage of the description of the correlation across color channels. The quality of the recovered secret image was improved, but at the cost of more bits to embed. Overall limitations for the above described methods often come from the number of bits needed to recover a secret image embedded in a mosaic image.

Aiming to reduce the number of transmitted bits when using mosaic image techniques, in this work we propose to modify the scheme in [12] for its application in DTT interactive applications. For this purpose, we use Kullback-Leibler Divergence (D_{KL}) [15] to determine the parametric probability density function (*pdf*) and associated parameters most appropriate to represent the distribution of the standard deviation in the secret image-blocks. Then, we estimate the position indices of the target image-blocks in the receiver by using the mosaic image information. A target image selection stage is subsequently performed by using the distributions of the image-block mean and standard deviation, together with their entropies, to identify a convenient target image among those available in a given multimedia application.

A specific experiment was addressed to characterize the entropy of the image-block means and standard deviations per color component, showing the usually close relationship among RGB components and revealing several informative uncorrelated cases. This motivated our proposal of a criterion to know in advance the suitability of an image as the most convenient target image, in comparison with the rest of images in the multimedia database. Finally, and by taking advantage of the preceding design and evaluation, the mosaic image can be advantageously created. For this analysis, a dataset of 20 different images was initially used in the experiments. These images were selected to represent different scenarios in terms of their variability in shape, texture or color. After this process, two images were selected as the best target images in this dataset, and a new 12-image dataset was collected by pursuing similar image properties in them, in order to finally evaluate the system performance. A very preliminary version of this work was presented in [16].

The structure of the paper is outlined as follows. In the next section, the notation and the data volume reduction on mosaic image techniques are presented. In Section III, the target image selection approach is introduced, and an improvement is proposed on the quality of the recovered secret image. In Section IV, our image dataset and the testbed configuration are presented. Besides, the conducted experiments and their results yield the parameters of the *pdf* of the block standard deviations, as well as the proposed criterion to identify the most appropriate target image. Finally, Section V contains conclusions and future perspectives.

II. DATA REDUCTION ON MOSAIC IMAGE TECHNIQUES

In this section, we establish the notation used throughout this work, and then we summarize the previous fundamentals of our proposal to reduce the data volume in mosaic image techniques. Figure 1 shows the outline of the involved procedure and images, which includes two main stages, namely, the mosaic image creation stage (in transmission), and the secret image recovery stage (in reception). The first stage (transmission) considers two images of the same size, namely, secret image S and target image T. The goal is to obtain a mosaic image M, as similar as possible to T, embedding the necessary bits to recover in the receiver an image that is very similar to S. For this purpose, a NRCT is first made on S and T according to [12] and [13]. Then, we propose here to take advantage of the distribution of some statistics extracted from the image blocks in S and T, and to construct a reduced-bit stream which can be embedded on M, hence obtaining M_T. In the second stage (reception), M_T can be separated in M and the bit stream, and M is also divided in blocks and some statistics are obtained from them. These values are used to estimate the same statistics of the blocks in T and to reverse the process applied in transmission, thus obtaining $\hat{S}$, which is a moderate-loss version of S.

Images are assumed to have the same size $v \times w$, and without loss of generality, we work here with 1024×768 size. The image blocks are denoted with capital letters and subindices, hence, secret image blocks set is $\{S_i\}_{i=1}^{b}$, and target image blocks set is $\{T_i\}_{i=1}^{b}$. Note that blocks do not overlap

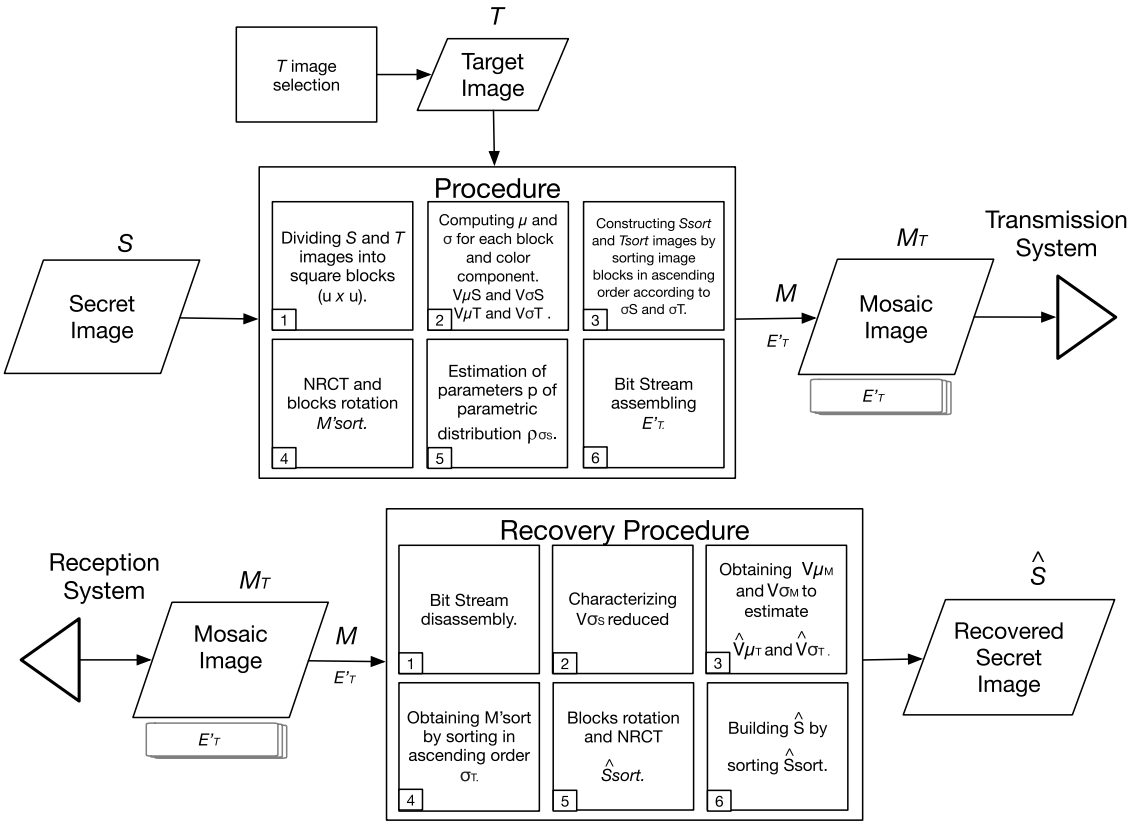

FIGURE 1. Outline for the use of Secret (*S*), Target (*T*), and Mosaic (*M*) images in the proposed procedure, both in transmission (upper panel) and in reception (bottom panel).

and subindices are extended according to

$$b = \left\lceil \frac{v \times w}{u \times u} \right\rceil \tag{1}$$

where u is the length of the block side, that usually is considered as 8, 16, or 32 pixels.

A. MOSAIC IMAGE CREATION

For a better understanding of the procedure, an example is presented in Figure 2 following the different stages. Secret image S and target image T are shown in Panels (a) and (b), respectively. They are divided into non-overlapping square blocks with size $u \times u$, providing a total of b blocks as given in Eq. (1). For a comprehensible visualization, $u = 256$ has been used to present image blocks $\{S_i\}_{i=1}^{b}$ and $\{T_i\}_{i=1}^{b}$ in Panels (c) and (d), respectively. For each block and color component (red, green, blue), average intensity (μ) and standard deviation (σ) values are computed, thus obtaining sets of $3b$ cardinality, i.e., sets V_{μ_S} and V_{σ_S} for the secret image, and sets V_{μ_T} and V_{σ_T} for the target image. Cardinality of sets V_{σ_S} and V_{σ_T} is reduced by averaging the three standard deviations associated to the three color components in the same image block, obtaining reduced sets $V^r_{\sigma_S}$ and $V^r_{\sigma_T}$. Then, the reduced sets are sorted in ascending order, providing the index vectors i_{σ_S} and i_{σ_T}. These vectors are used to sort blocks in S and T accordingly, yielding images S_{sort} (see Panel (e)) and T_{sort}. The next step is to apply the NRCT color transfer scheme so that the color components of image S_{sort} are as similar as possible to those of T_{sort}.

Thus, for any color component $c = \{r, g, b\}$, the following transformation is applied to pixels in the *i-th* image-block of S_{sort},

$$c^c_{M_{sort_i}} = q_{c,i}\left(c^c_{S_{sort,i}} - \mu^c_{S_{sort,i}}\right) + \mu^c_{T_{sort,i}} \tag{2}$$

for $i = 1, \cdots, b$. Variables $\mu^c_{S_{sort,i}}$ and $\mu^c_{T_{sort,i}}$ are the average intensity for pixels in component c of the $i-th$ block images S_{sort} and T_{sort}, respectively. Variable $q_{c,i}$ is the standard deviation quotient, obtained as

$$q_{c,i} = \sigma^c_{T_{sort,i}} / \sigma^c_{S_{sort,i}} \tag{3}$$

for $i = 1, \cdots, b$, and where $\sigma^c_{S_{sort,i}}$ and $\sigma^c_{T_{sort,i}}$ is the standard deviation for values in component c of the $i-th$ image block in S_{sort} and T_{sort}, respectively. The resulting image is denoted as M_{sort}. This process is performed to get better edges definition in the mosaic image, and in our work also to support the contribution to the new parametrization presented in Section II-B. Following the scheme in [12], every block of M_{sort} is rotated four angles {0, 90, 180, 270}. For each block of M_{sort}, we select the angle associated to the minimum Root Mean Square Error (RMSE) between the rotated block and the block of T_{sort} in the same position, thus obtaining the vector of rotation angles named V_θ. Image M'_{sort} is obtained by applying rotation angles in V_θ to blocks in M_{sort}, as shown

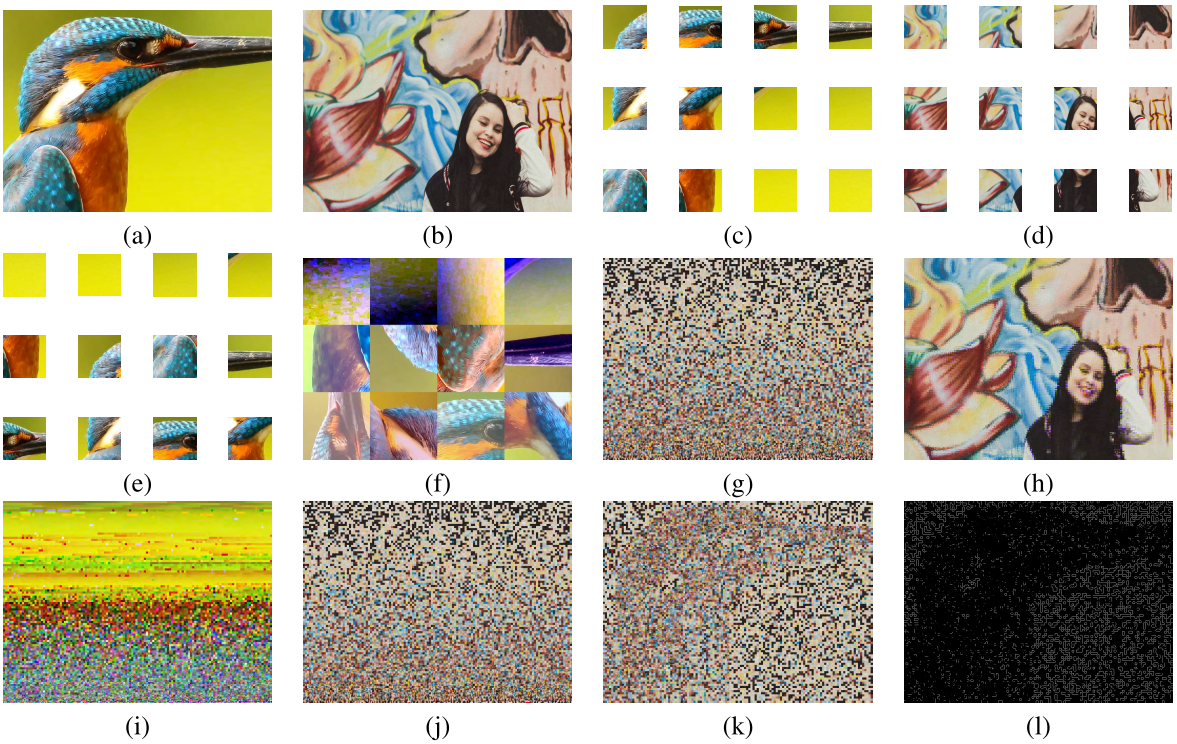

FIGURE 2. Process to create the mosaic image: (a) Secret image S; (b) Target image T; (c) Division of S in blocks with $u = 256$; (d) Division of T in blocks with $u = 256$; (e) S_{sort} using $u = 256$; (f) and (g) M'_{sort} using $u = 256$ and $u = 8$, respectively; (h) Mosaic image M, created from (a) and (b) when $u = 8$. An example of wrong block-rearranging in M'_{sort} is also shown: (i) S_{sort} using $u = 8$; (j) M'_{sort} using $u = 8$; (k) Rearranging M'_{sort} using i_{σ_S}; (l) Binary edges of image in (k).

in Figure 2 (f) for $u = 256$ and in Panel (g) for a more realistic situation with $u = 8$. Finally, Panel (h) shows mosaic image M after the rearrangement of blocks in M'_{sort} using position indices i_{σ_T}. Note that M looks very similar to target image T.

The importance of the block reordering in M'_{sort} to construct M is also illustrated in Figure 2 when $u = 8$. For this purpose, Panel (i) is the equivalent image to Panel (e) with a reduced block size, and Panel (j) is the same as Panel (g). When performing a different re-ordering of the image blocks in Panel (j), the obtained mosaic image is very different to T. This can be observed in Panel (k), which has considered indices in i_{σ_S} instead of those in i_{σ_T}. This intentionally wrong rearrangement of blocks in M'_{sort} makes the bird shape (secret image) to appear in the new mosaic image. Only for better understanding, binary edges of image in Panel (k) are shown in Panel (l).

Since the final aim is to embed relevant information into M, the next stage is to construct bit stream E_T to be embedded. Li and Tsai [12] proposed to create E_T as a concatenation of b bit streams $\{E_i\}_{i=1}^{b}$ to recover $\{S_i\}_{i=1}^{b}$. The bit stream for each block consists of five components, given by

$$E_i = [t_1 t_2 ... t_n]_i [r_1 r_2]_i [m_1 m_2 ... m_{48}]_i [q_1 q_2 ... q_{21}]_i [d_1 d_2 ... d_k]_i \tag{4}$$

for $i = 1, \cdots, b$, and where bit segment $[t_1 t_2 ... t_n]_i$ codes the value of index vector i_{σ_T} associated to the $i-th$ block, with $n = \lceil log_2(b) \rceil$; bit segment $[r_1 r_2]_i$ codes the rotation angle and needs two bits because there are four possible rotation directions; bit segment $[m_1 m_2 ... m_{48}]_i$ has 48 bits to represent the means of every component in S_i and T_i, 8 bits per color component; bit segment $[q_1 q_2 ... q_{21}]_i$ codes the standard deviation quotients with 21 bits, 7 bits per color component; and segment $[d_1 d_2 ... d_k]_i$ uses k bits to code the residuals, depending on the number of overflows and underflows. Residuals were also considered in [12], and they were handled by using Huffman coding, but they are not considered in the present work, so this detail has to be borne in mind in the comparisons and experiments.

B. PROPOSED DATA REDUCTION

In order to reduce the number of bits required in [12], we propose to eliminate from E_i the bit segments involving data from the target image (i.e., t, q, d, and part of m). The resulting bit stream is as follows:

$$E'_i = [r_1 r_2]_i [m_{sort_1} m_{sort_2} ... m_{sort_{24}}]_i [s_1 s_2 ... s_n]_i \tag{5}$$

for $i = 1, \cdots, b$, and where bit segments $[r_1 r_2]_i$, $[m_{sort_1} m_{sort_2} ... m_{sort_{24}}]_i$ and $[s_1 s_2 ... s_n]_i$ code the rotation angle, the average intensity per component, and the value of the index vector i_{σ_S} of block S_i, respectively. Average intensities in V_{μ_S} are sorted by vector i_{σ_S}, therefore, they are denoted in the bits segment with m_{sort}. To compensate for this reduction in the bit stream, we propose several contributions.

Our first contribution includes into the reduced bit stream a few number of bits to code parameters p_{σ_S} of the parametric

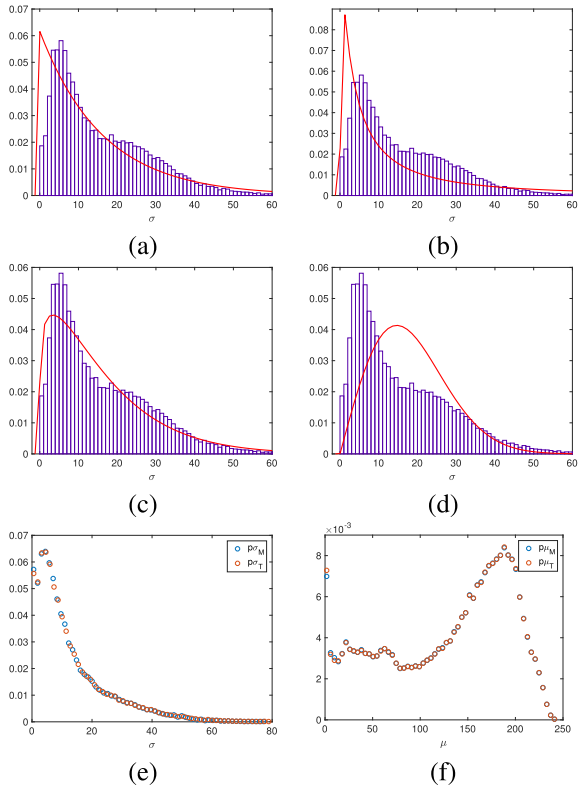

FIGURE 3. Normalized histograms of σ_S (in blue) and the best fit for parametric distributions (in red): (a) Exponential; (b) Log-normal; (c) Weibull; (d) Rayleigh. Also the empirical mean and standard deviation distributions are shown for target and mosaic image blocks, (e) ρ_{σ_M} vs. ρ_{σ_T}; (f) ρ_{μ_M} vs. ρ_{μ_T}.

distribution best representing the empirical distribution of $V^r_{\sigma_S}$ (denoted as ρ_{σ_S}). For this purpose, a predefined set of parametric *pdfs* were considered, namely, Exponential, Log-normal, Weibull, and Rayleigh. The best parameters for each *pdf* were found according to the maximum likelihood criterion and considering the three color components altogether. As an example, panels (a)-(d) in Figure 3 show the normalized histogram of $V^r_{\sigma_S}$ (in blue) and the best approximation for every parametric distribution (in red). The D_{KL} was used to select the best choice, and parameters p_{σ_S} were also used in reception to estimate Eq. (3).

Then, the new E'_T bit stream is the concatenation of bit streams E'_i ($i = 1 \cdots b$) and bit segment coding parameters p_{σ_S}. Bit stream E'_T is now obtained as

$$E'_T = \bigcup \{E'_i\}_{i=1}^{b} s_1 s_2 ... s_p, \tag{6}$$

where $\bigcup$ represents the segments concatenation, and s_p is the number of bits to code p_{σ_S}. As we do not transmit all the bits of Eq. (4), our second contribution takes advantage of the similarity between M and T images to estimate in reception the sets V_{μ_T} and V_{σ_T} using M, which together with E'_T, are required to estimate $\hat{S}'$. Figure 3 also depicts the similarity between empirical distributions $\rho_{\sigma_M} \approx \rho_{\sigma_T}$ and $\rho_{\mu_M} \approx \rho_{\mu_T}$, in Panels (e) and (f), respectively.

For transmission, E'_T can be embedded into M by the LSB replacement method used in [12] to obtain image M_T. Note that the mentioned previous works inserted the bit stream in the mosaic image, whereas we are considering that our bit stream can be sent by the data channel in a number of different multimedia applications. Nevertheless, the comparison in terms of the number of required bits can be informative in terms of the reported performance herein.

C. SECRET IMAGE RECOVERY

Also following [12], both bit stream E'_T and mosaic image M can be obtained from M_T. In summary, the stream E'_T is segmented to get parameters p_{σ_S} characterizing the empirical distribution of $V^r_{\sigma_S}$, the rotation angle of every block in M'_{sort} (from $\{[r_1 r_2]_i\}_{i=1}^{b}$), the mean value $\mu^c_{S_{sort}}$ for every block and color component in S_{sort} (from $\{[m_{sort_1} m_{sort_2} ... m_{sort_{24}}]_i\}_{i=1}^{b}$), and the index vector i_{σ_S} (from $\{[s_1 s_2 ... s_n]_i\}_{i=1}^{b}$). Then, we randomly generate b values according to the selected parametric distribution using parameters p_{σ_S}. These values are sorted in descendant order and assigned to the standard deviation of blocks obtaining $\hat{V}_{\sigma_{S_{sort}}}$. According to the second contribution presented in Section II-B, sets V_{μ_M} and V_{σ_M} are estimated as $\hat{V}_{\mu_T}$ and $\hat{V}_{\sigma_T}$, because of the similarity between T and M images. By averaging the standard deviations associated to the three color components in the same image block, we obtain from V_{σ_M} the reduced set $V^r_{\sigma_M} = \{\sigma_{M,i}\}_{i=1}^{b}$. Values in $V^r_{\sigma_M}$ are sorted in ascending order, providing the vector of indices i_{σ_M} necessary to construct M'_{sort}. Next, the $i-th$ block in M'_{sort} is rotated in the reverse direction using V_θ to form M_{sort}.

After previous steps, we have the information to estimate $\{\hat{S}_i\}_{i=1}^{b}$, i.e. the blocks of an estimation of the secret image. For this purpose, we first apply a color conversion process similar to that in transmission, so that pixels in blocks of M_{sort} have similar statistics to those in corresponding blocks of $\hat{S}_{sort}$. Thus, for every block we obtain quotient $q_{r,i}$ as

$$q_{r,i} = \frac{\hat{\sigma}_{\hat{S}_{sort},i}}{\sigma_{M,i}} \tag{7}$$

for $i = 1, \cdots, b$, which, together with the mean values $\mu^c_{M_{sort},i}$ and $\mu^c_{S_{sort},i}$, is used to find pixel values $c^c_{\hat{S}_{sort},i}$ for every color component $c = \{r, g, b\}$ in $\hat{S}_{sort}$ according to

$$c^c_{\hat{S}_{sort},i} = q_{r,i}\left(c^c_{M_{sort},i} - \mu^c_{M_{sort},i}\right) + \mu^c_{S_{sort},i} \tag{8}$$

where $c^c_{M_{sort},i}$ and $\mu^c_{M_{sort},i}$ are the $c-th$ component of pixels in M_{sort} and the average intensity for the i-th block of M_{sort}, respectively.

Finally, we build image $\hat{S}$ by rearranging blocks of $\hat{S}_{sort}$ according to indices i_{σ_S}.

III. PROPOSED METHOD FOR TARGET IMAGE SELECTION

Many multimedia applications work with an image set that could be naturally used as possible target images, like in digital interactive television, military image databases, or medical imaging systems. This is often the case of applications in systems ensuring the total reception of data with parity check process. Therefore, we propose a method that can be used

for target image selection in this kind of scenarios. In general terms, the content of an image can be described by features like shape, texture, or color. Due to the use of image blocks in the method proposed so far, it has been previously determined that color is the most effective feature, given that it affects the overall visual appearance of the resulting mosaic image. We focus now on the statistical characteristics (μ and σ) of the color distributions from images-blocks in order to define a similarity measure to be used in the target image selection.

Entropy is defined as the weighted average value of the amount of information, which represents a measure of the average uncertainty about a random variable x, and then about the amount of information in it [17]. The entropy of x is obtained as follows,

$$h(x) = -\int_{-\infty}^{\infty} \rho(x) log_2 \rho(x)\, \mathrm{d}x, \tag{9}$$

where $\rho(x)$ is the *pdf* of x. In our case, we work with random variables ρ_{σ_S}, ρ_{σ_T}, ρ_{μ_S}, and ρ_{μ_T}, whose entropies are denoted as $h(\sigma_S)$, $h(\sigma_T)$, $h(\mu_S)$, and $h(\mu_T)$. The usefulness of entropy to define image characteristics has been widely studied in the literature. Pluim *et al.* [18], Skilling and Gull [19], Lee *et al.* [20], and Zhao *et al.* [21] different areas use it for image processing via maximum entropy methods or to register satellite images by block processing via entropy, among others. Therefore, the entropy of the intensity levels of each RGB component of the image can be used in the comparisons between images. An image consisting of almost a single intensity level will have a low entropy value and it contains very little information. A high entropy value will be yielded by an image with uniform quantities of many different intensity levels, which is an image containing a lot of information. In this manner, the entropy is also a measure of dispersion of a random variable (the intensity level in our setting).

One could think of addressing the process of recovery of the S image with the T images by using a one-versus-all calculation. However this would become non-operative from a practical viewpoint. Therefore, our goal now is to create a target-image selection stage, and we hypothesize that the entropy of different statistical parameters of the image-blocks could be used as a quantitative criterion for this stage. To this aim, we empirical analyze the described entropies and their relation with several quality measurements on the $\hat{S}$. From the experimental analysis presented in detail in Section IV-D, we define the criterion by concluding that the most appropriate images to be chosen as target images are those with values of $h(\mu) \in (7.2, 7.6)$ and $h(\sigma) \in (4.3, 4.8)$), respectively. In our problem, we look for the specific image characteristics that can help us to select the appropriate target image under that quantitative criterion. Figure 4 shows examples of the histograms of V_μ^r and V_σ^r for three different images, together with their $h(\mu)$ and $h(\sigma)$ values. It can be visually noticed therein the direct relation between the entropy and the image statistic dispersions, i.e., the lower the entropy, the lower the block statistic dispersion and vice-versa. This qualitative observation will be further scrutinized in the experiments.

Let us denote the secret image that we want to embed by S^o, and the set of K_T available target images in the system by $\{T^k\}_{k=1}^{K_T}$. After embedding S^o into a given T^k, we eventually recover an estimated version denoted by $\hat{S}^{o,k}$. The previously explained procedure can be compactly denoted by operator Θ, as follows:

$$\hat{S}^o = \Theta\left(S^o, \{T^k\}_{k=1}^{K_T}\right). \tag{10}$$

Then, the estimation error is given by

$$Err = \Phi\left(S^o, \hat{S}^o\right) \tag{11}$$

where operator Φ denotes the quantitative quality measurement of the reconstructed secret image in comparison with the original one. The *Err* measurement can be here either the RMSE or the Mean Structural Similarity (MSSIM). The former quality measurement is a quantitative performance one, and it assesses how well a method performs to reconstruct an image relative to the original one, meanwhile the latter is used to determine the perceived and subjective quality, in terms of the structural information between a recovered image and the original one.

We are looking for an alternative criterion based on entropies $h(\mu)$ and $h(\sigma)$ for each color component, which we denote here as Λ operator. This operator is to be determined in such a way that it allows us to identify the best image T_{opt}^o among the available target ones that fits to embed our secret image, without the need of using the operator Φ in all the cases, this is,

$$T_{opt}^o = \Lambda\left(S^o, \{T^k\}_{k=1}^{K_T}\right). \tag{12}$$

Accordingly, Λ operator should be designed to be capable of *a priori* identifying which target image is appropriate for our secret image, but only by performing simple calculations of the entropy of the image statistics in the target image available database. Based on the above description, T_{opt}^o is the target image that reduces to a minimum the error between the S image and the $\hat{S}$ image. The detailed algorithm for target image selection is described as Algorithm 1.

IV. EXPERIMENTS AND RESULTS

Several experiments were performed in order to create and test the proposed method. First, for a better presentation of the experiments, we introduce in this section the image sets. Then, the number of bits required to estimate S from M was scrutinized in order to reduce it. For this purpose, a parametric description of ρ_{σ_S} was obtained together with an estimation of empirical distributions ρ_{σ_T} and ρ_{μ_T}. Finally, the suitability of selecting the best T image with entropy criteria was analyzed.

A. SET OF IMAGES

For this work we compiled a set of 20 high-quality JPG color images freely accessible and maybe of use in multimedia applications. Images were cropped to work at one of the

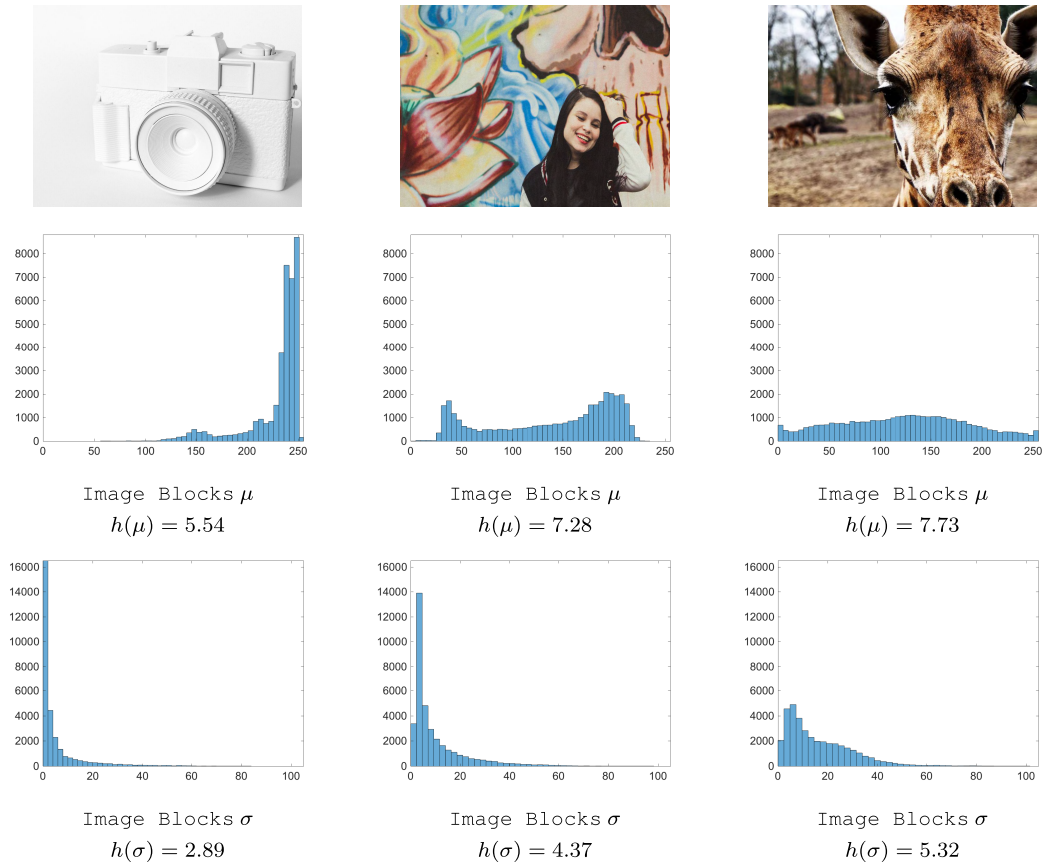

FIGURE 4. Histograms of V_μ^r and V_σ^r from three different images, with their corresponding entropy values $h(\sigma)$ and $h(\mu)$.

Algorithm 1 Target Image Selection

Input: secret image S^o, and target image set $\{T^k\}_{k=1}^{K_T}$
Output: the more suitable target image T_{opt}^o.

Step 1. Divide target images $\{T^k\}_{k=1}^{K_T}$ into b blocks, with b as given in Eq. (1).
Step 2. Compute the average intensity (μ) and standard deviation (σ) values for each block and color component, obtaining V_{μ_T} and V_{σ_T} sets of $3b$ cardinality.
Step 3. Compute the entropy of each set V_{μ_T} and V_{σ_T}, getting $h(\mu)$ and $h(\sigma)$ for each color component.
Step 4. Check accomplishment of the criterion based in entropy values for $h(\mu)$ and $h(\sigma)$.
Step 5. Select the most suitable target image T_{opt}^o.

typical resolutions for screen presentation, 1024×768 pixels. All the images in this work were obtained from the Internet [22]. In Figure 5 we show the images in alphabetic order (from *Image A* to *Image T*) from top to bottom and from left to right.

In order to carry out an operational number of experiments, we worked with 190 image combinations in the following way. We used ten possible secret images (from *Image A* to *Image J*), and all the set of images as target ones, considering that the same image was not used as secret and target at a time. As an example, the first experiment is carried out by using *Image A* as secret image and the remaining 19 as target images.

After identification of the possible T_{opt}^o images in that set using the Algorithm 1, a new set of 12 images (Figure 6) was collected from the same source [22], to be used as target ones in Section IV-C and thereafter. The selection of this set of images was more specific this time, as it was based on the simple calculations of the entropy related to Eq. (12). With this new dataset, we analyzed how the quality of the recovered image increased when using the same secret images as those in the previous set.

B. IDENTIFICATION OF THE DISTRIBUTION AND THE ASSOCIATED PARAMETERS FOR ρ_{σ_S}

In this experiment we determine the parametric distribution (ρ_{pdf}) best representing the empirical distribution ρ_{σ_S} among the following: Exponential, Log-normal, Weibull, or Rayleigh. After, we construct the ρ_{σ_S} using each possible image T, and we determine the best parameters for each parametric distribution according to the maximum likelihood criterion. The $D_{KL}(\rho_{\sigma_S}||\rho_{pdf})$ was calculated to determine the best parametric distribution in each case. This provided a non-symmetric measure of dissimilarity or difference between distributions ($D_{KL}(\rho_{\sigma_S}||\rho_{pdf})$ is different

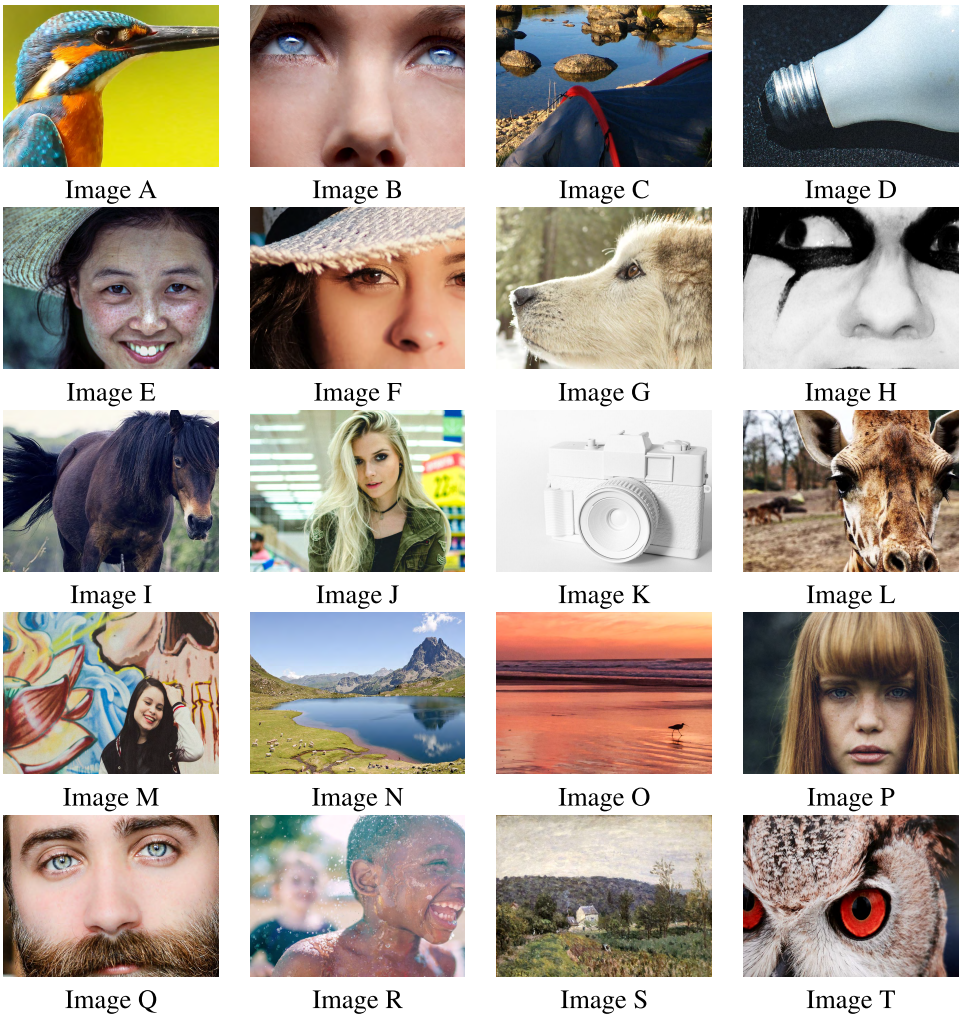

FIGURE 5. Set of used images. We denoted them from left to right and from top to bottom with capital letters from A to T (e.g., *Image A* is the bird one, and *Image T* is the owl one).

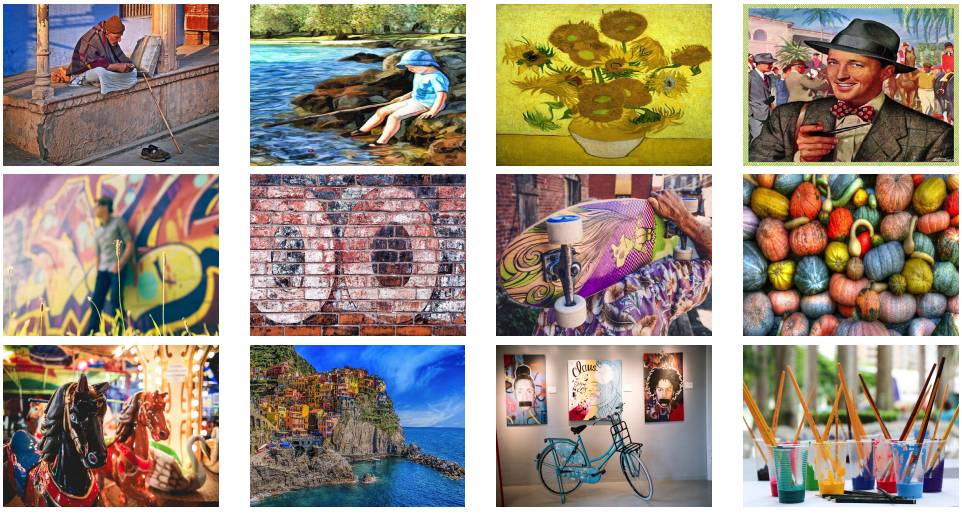

FIGURE 6. Set of images collected according to the identified characteristics.

to $D_{KL}(\rho_{pdf}||\rho_{\sigma_S})$). Note that distributions are more similar when D_{KL} is closer to zero. The values of D_{KL} between the empirical distributions of each image and the scrutinized parametric distributions are shown in Table 1. The values of D_{KL} representing the closest similarity are shaded in gray, and the second closest D_{KL} are in green.

TABLE 1. Kullback Leibler Divergence (D_{KL}) for the parametric distributions (*pdf*, first row) when considering the first image dataset (first column). The values of D_{KL} representing the closest similarity are shaded in gray, and the second closest D_{KL} are in green.

	Exponential		Log-normal		Weibull		Rayleigh	
	$D_{KL}(\rho_{\sigma_S}\|\|\rho_{pdf})$	$D_{KL}(\rho_{pdf}\|\|\rho_{\sigma_S})$	$D_{KL}(\rho_{\sigma_S}\|\|\rho_{pdf})$	$D_{KL}(\rho_{pdf}\|\|\rho_{\sigma_S})$	$D_{KL}(\rho_{\sigma_S}\|\|\rho_{pdf})$	$D_{KL}(\rho_{pdf}\|\|\rho_{\sigma_S})$	$D_{KL}(\rho_{\sigma_S}\|\|\rho_{pdf})$	$D_{KL}(\rho_{pdf}\|\|\rho_{\sigma_S})$
A	0.52	0.46	0.61	0.01	0.46	0.01	1.32	3.16
B	0.32	0.11	0.01	0.05	0.38	0.11	0.80	1.25
C	0.41	0.24	0.11	0.12	0.64	0.21	0.84	1.26
D	1.21	0.69	0.57	0.46	0.91	0.65	0.94	0.95
E	0.27	0.06	0.08	0.05	0.08	0.03	0.25	0.34
F	0.29	0.21	0.62	0.22	0.37	0.12	1.11	2.28
G	0.20	0.04	0.04	0.06	0.05	0.01	0.19	0.31
H	0.21	0.06	0.15	0.01	0.45	0.01	0.81	1.34
I	0.12	0.02	0.44	0.22	0.08	0.02	0.21	0.49
J	0.09	0.01	0.31	0.12	0.08	0.01	0.53	0.87
K	7.95	1.30	14.71	0.30	10.80	0.44	3.51	7.00
L	0.18	0.06	0.15	0.12	0.04	0.02	0.17	0.24
M	0.76	0.24	0.15	0.11	0.63	0.24	0.54	0.81
N	0.38	0.39	0.34	0.29	0.67	0.30	0.70	1.55
O	0.22	0.07	0.01	0.06	0.28	0.06	0.58	0.94
P	0.46	0.09	0.02	0.04	0.09	0.04	0.17	0.23
Q	0.22	0.14	0.11	0.12	0.37	0.12	0.55	1.02
R	0.19	0.04	0.07	0.07	0.13	0.03	0.35	0.54
S	3.27	0.26	0.06	0.04	0.31	0.09	0.15	0.13
T	0.13	0.05	0.11	0.15	0.03	0.01	0.16	0.23

We can see that the Rayleigh *pdf* is systematically misfit and never gets the best or the second best positions in the conducted experiments, so that it is ruled out from now on. The Log-normal *pdf* is the one which most adheres to our ρ_{σ_S} distribution, with 12 (3) out of 20 results in advantage (second choice). If the Log-normal *pdf* was not used, then the second possibility should be the Weibull (6 and 7) or the Exponential (2 and 10 as first and second, respectively) *pdf*. We checked that the use of any of the second options instead of the Log-normal *pdf* would represent in general a quality decrease of the final recovery, which is not very considerable in quantitative terms, but possible to detect visually. We also checked that the Log-normal *pdf* works better on images with high dispersion in the standard deviation of the image-block, whereas the Weibull and Exponential ones suit better to images with lower dispersion.

To confirm the Log-normal *pdf* as the most convenient distribution to be used in our system, we further analyzed subjectively several special cases, specifically, those in which the Log-normal *pdf* was not the first option in Table 1. In this setting, 4 groups were identified: (Group 1) Exponential *pdf* as first option and Log-normal *pdf* as second option; (Group 2) Weibull *pdf* as first option and Log-normal *pdf* as second option; (Group 3) Weibull *pdf* as first option and Exponential *pdf* as second option; And (Group 4) Exponential *pdf* as first option and Weibull *pdf* as second option. In Figure 7, we can see the approximation of the ρ_{σ_S} distribution (in blue) towards the closest *pdf* (in yellow) according to defined groups, and the Log-normal *pdf* (in red). The Log-normal *pdf* was not very far from the adjustments corresponding to each closest case, therefore it can be considered to be still good-enough to parametrize ρ_{σ_S}.

Once decided that the Log-normal *pdf* is used to model ρ_{σ_S}, we determine its parameters. Each parameter is assigned to

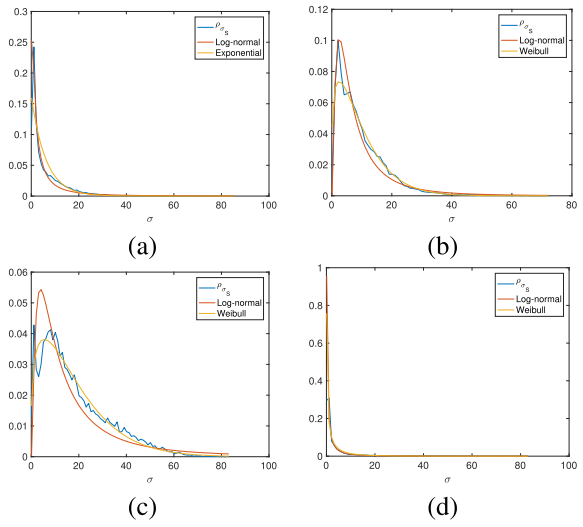

FIGURE 7. Special cases on fit quality of ρ_{σ_S} to several parametric distributions: (a) Results for the F image (group 1); (b) Results for the G image (group 2); (c) Results for the T image (group 3); (d) Results for K image (group 4).

the nearest unsigned integer, so that 16 bits are needed (8 per parameter), and we insert them in the stream E'_T as described in Eq. (6). Recall that E'_T could be embedded into image M in transmission to obtain image M_T to be sent. This stream is extracted from M_T in reception, to allow the recovery process of the secret image. It is important to emphasize at this point that the experiments here performed have been considered for scenarios with high signal-to-noise ratio (an expected situation in DTT applications) with quality-control handling. This means that the multimedia application will not present the image until it has received all the packages related to it, in order to perform the decoding process. Just for a comparison in the processing time for transmission, we also checked

TABLE 2. $D_{KL}(\rho_{\mu_M}||\rho_{\mu_T})$ and $D_{KL}(\rho_{\sigma_M}||\rho_{\sigma_T})$ for T images with their respective M images (for the first experiment using Image A as secret one, and for Image A as target we use Image B as secret).

T/M image	A	B	C	D	E	F	G	H	I	J
ρ_μ	0.0156	0.0155	0.0153	0.0295	0.0071	0.0201	0.0265	0.0102	0.0216	0.0117
	0.0046	0.0296	0.0049	0.0070	0.0010	0.0092	0.0033	0.0040	0.0084	0.0071
ρ_σ	0.0022	0.0027	0.0054	0.0014	4.31×10^{-4}	3.85×10^{-4}	4.9×10^{-4}	9.7×10^{-4}	6.1×10^{-4}	0.0032
	0.0020	0.0014	0.0053	0.0014	4.32×10^{-4}	3.84×10^{-4}	4.8×10^{-4}	9.8×10^{-4}	6.2×10^{-4}	0.0031
T/M image	**K**	**L**	**M**	**N**	**O**	**P**	**Q**	**R**	**S**	**T**
ρ_μ	0.0339	0.0398	0.0162	0.0284	0.0065	6.6×10^{-4}	0.0507	0.0060	0.0293	0.0309
	0.0040	0.0052	0.0036	0.0078	0.0022	6.5×10^{-4}	0.0075	0.0059	0.0149	0.0070
ρ_σ	0.0025	9.65×10^{-4}	0.0032	0.0030	0.0034	1.87×10^{-4}	0.0013	7.23×10^{-4}	0.0037	0.0012
	0.0025	9.61×10^{-4}	0.0012	0.0030	0.0032	1.87×10^{-4}	0.0012	7.02×10^{-4}	0.0037	0.0012

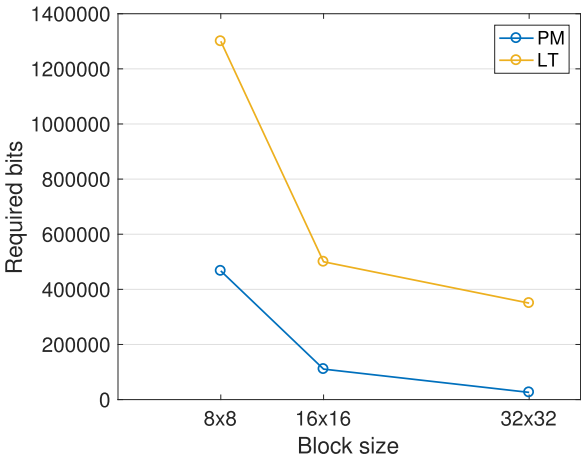

FIGURE 8. Results of data reduction, number of bits required to retrieve a S image S, and comparison between the proposed method (PM) and the method of *Li and Tsai* (LT) [12].

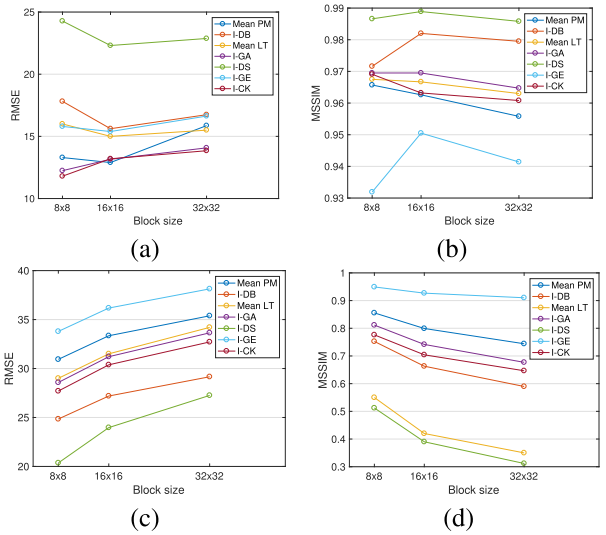

FIGURE 9. Performance results in terms of RMSE and MSSIM. PM stands for Proposed Method, LT stands for Li and Tsai method, and some experiments randomly selected represented as Images-SecretTarget. (a) RMSE between $\hat{S}$ and S images for different block sizes (8×8, 16×16, 32×32); (b) MSSIM between $\hat{S}$ and S images; (c) RMSE between M and T images; (d) MSSIM between M and T images.

that the time devoted by our approach is similar to that by the Li and Tsai technique.

C. ESTIMATING THE T IMAGE PARAMETERS BASED ON THE M IMAGE PARAMETERS

In order to further reduce the amount of bits to embed into M, we took advantage of the similarity between images M and T (see Section II-B) and estimated the block statistics μ_T and σ_T at reception. Using the D_{KL}, we determined a strong similarity between ρ_{σ_M} and ρ_{σ_T}, and between ρ_{μ_M} and ρ_{μ_T}, for all images that acted as a T image, and for their respective M images obtained in Section II-A. In Table 2 we present as example the D_{KL} obtained between the distributions corresponding to T and M for the experiment where Image A is the secret one (for Image A as target we use Image B as secret), which supports the strong similarity of $\rho_{\sigma_M}/\rho_{\sigma_T}$ and $\rho_{\mu_M}/\rho_{\mu_T}$ distributions, and corroborates the good functionality of the NRCT process when considering information related to μ and σ in Eq. (2) and Eq. (3).

By putting together the experiments in Sections IV-B and IV-C, we present in Figure 8 the results of reducing the number of bits required. Results of our approach are in blue line (PM stands for Proposed Method) and results of *Li and Tsai* method [12] are in yellow line (LT stands for Li and Tsai method). The number of required bits is dramatically decreased (close to 3 to 1) with respect to the results in *Li and Tsai* work [12]. Also, the smaller the u value, the larger the required number of bits and the more functional reduction ratio of our approach.

Several performance measurements were considered to evaluate the differences between the $\hat{S}$ and the S images, and also between the M and the T images. Figure 9(a-d) shows the performance results, in terms of both RMSE and MSSIM, by considering the average of the 190 experiments. Average results of our approach are in blue line, besides, we also plotted the average results in Li and Tsai [12] (yellow lines), and some experiments randomly selected (represented as **I**mages-**S**ecret**T**arget. i.e. I-GA stands for experiment with Image G as Secret image and Image A as Target image).

In Panel (a), the RMSE values of the recovered secret images with respect to the original ones show that our method has an average RMSE below $\simeq 15$, which is subjectively acceptable. The MSSIM values of the recovered secret images with respect to the original ones when considering different block image sizes are shown in Panel (b), and it varies from $\simeq 0.95$ to $\simeq 0.97$ in average. This shows the

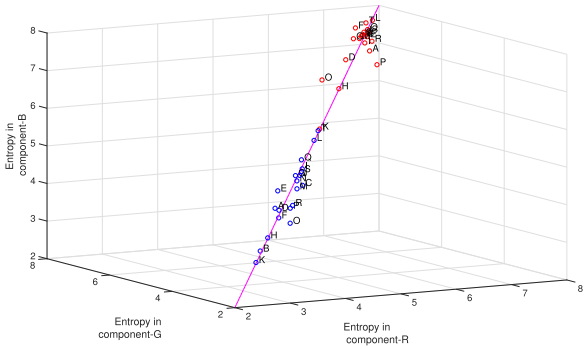

FIGURE 10. Block entropy values $h(\mu)$ and $h(\sigma)$ (red and blue points), jointly represented for RGB color components of the first image database using $u = 8$. Magenta-colored line represents the region with the same block-entropy for each color component.

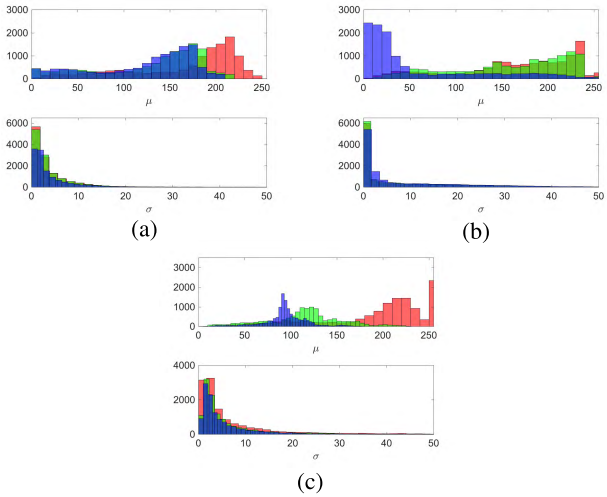

FIGURE 11. Normalized histograms for the special cases in the relation $h(\mu)$ and $h(\sigma)$ vs. V_σ and V_μ, respectively: (a) Image B histograms; (b) Image A histograms; (c) Image O histograms.

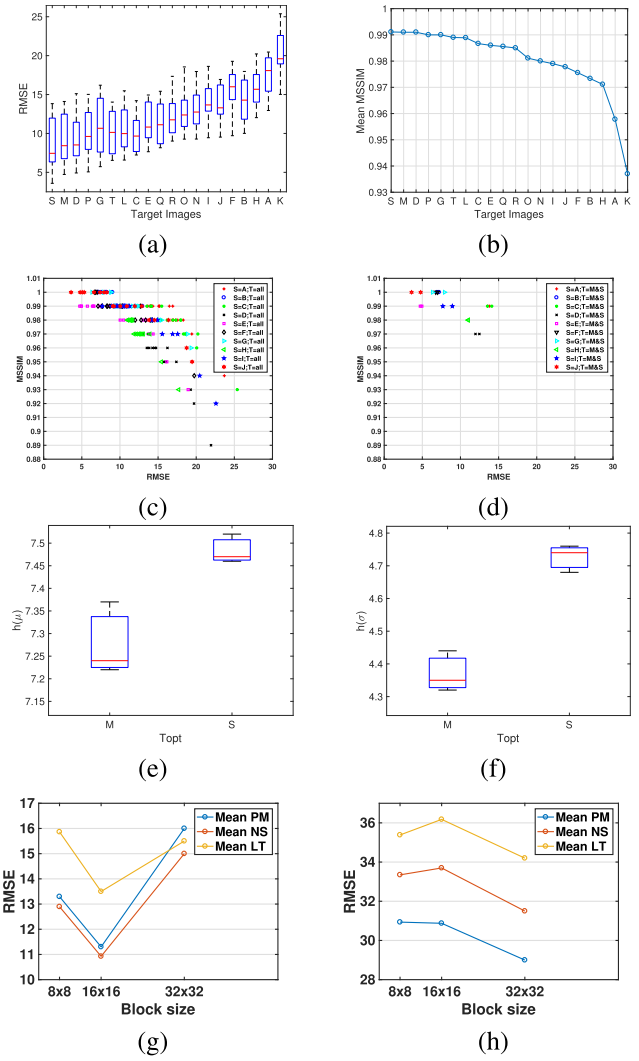

FIGURE 12. Entropy criterion analysis: Summary statistics when comparing S and $\hat{S}$ generated with all T images, considering (a) RMSE; (b) mean MSSIM; (c) RMSE and MSSIM using the whole set of images as target; (d) RMSE and MSSIM using only *Image S* and *Image M* as target; (e) Summary statistics for entropies $h(\mu)$ in *Image S* and *Image M*; (f) Summary statistics for entropies $h(\sigma)$ in *Image S* and *Image M*; Performance results in terms of RMSE and MSSIM. PM stands for Proposed Method, LT stands for Li and Tsai method, and NS stands for New Set. (g) Mean RMSE between S and $\hat{S}$ working with target images coming from the new image set; (h) Mean RMSE between M and T working with target images coming from the new image set.

good similarity of the details of the recovered secret image with those of the original ones. Likewise, the RMSE values of the mosaic images with respect to the target images are shown in Panel (c), in which the mosaic image yielded by the proposed method has RMSE below $\simeq$ 35 with respect to the target image. It can be seen from these panels that the mosaic image retains more details of the target image when u (the block size) is smaller. Hence, a mosaic image created with smaller u value has smaller RMSE with respect to the target image, what seems to be reasonably expected. Panel (d) shows the MSSIM values of the mosaic images with respect to the target images for different block sizes. Note that MSSIM varies from $\simeq$ 0.75 to $\simeq$ 0.87 in average, showing the high similarity between mosaic and target images.

D. SELECTING MORE SUITABLE T IMAGES USING ENTROPY ANALYSIS

Figure 10 depicts a 3-dimensional representation of the entropy values for each color component (in RGB) when considering blocks of size 8×8. The entropy values from V_μ (red points) and V_σ (blue points) are represented for all the images in the first dataset. We can distinguish three different groups according to the entropy variation of the block mean ($5.5/5.5/5.5 < h(\mu) < 7.8/7.8/7.7$) and the standard deviation ($2.9/2.9/2.9 < h(\sigma) < 5.5/5.5/5.5$) per color component. First, a group of images with low entropy values are related to low information dispersion, which means that they tend to have slight intensity variation. Images D (with $h(\mu) = 6.8/6.9/6.9$ and $h(\sigma) = 3.9/3.9/4.0$), H (with $h(\mu) = 6.3/6.3/6.3$ and $h(\sigma) = 3.4/3.4/3.4$), and K (with $h(\mu) = 5.5/5.5/5.5$ and $h(\sigma) = 2.9/2.9/2.9$) are in this group. Second, images with high entropy values are closely related to high information dispersion. In this group we find cases with a very broad range of colors, and with

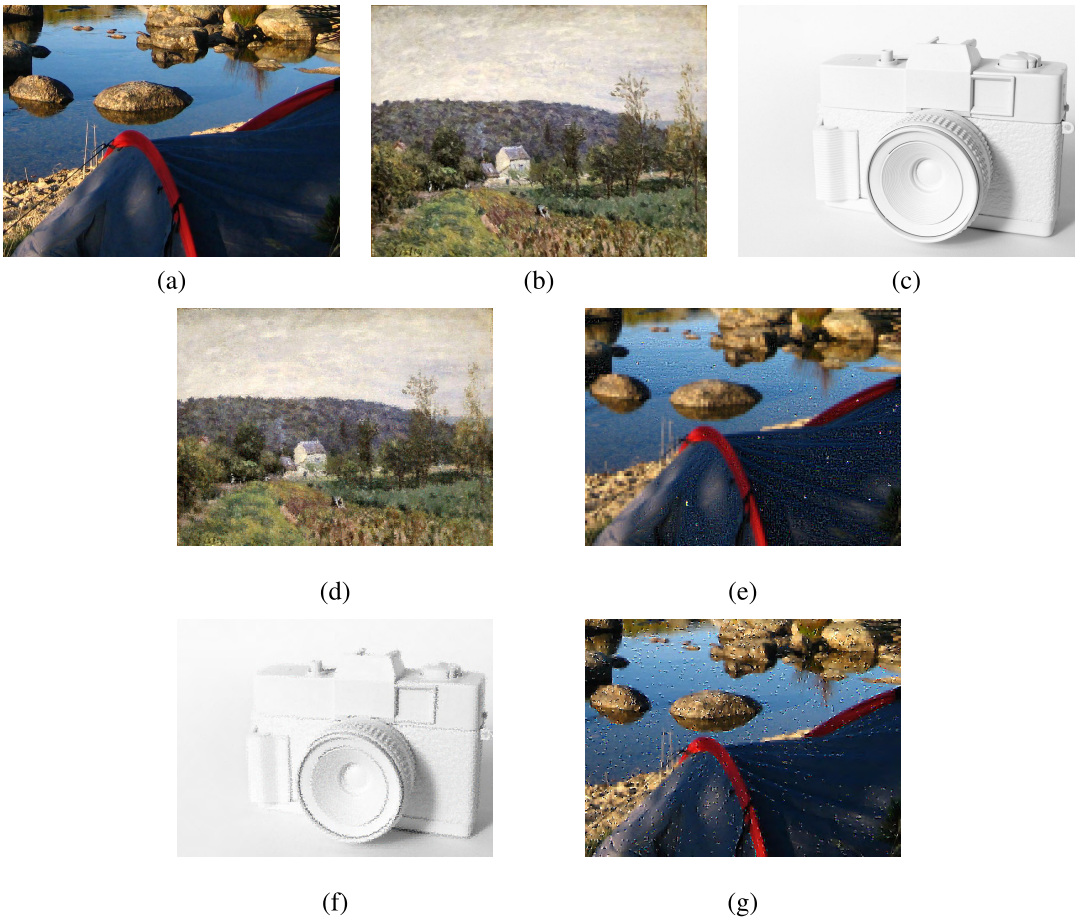

FIGURE 13. Mosaic and recovered images with the same secret image (using $u = 8$). (a) Secret image; (b) Target image One; (c) Target image Two; (d) and (f) Mosaic images, and (e) and (g) Recovered secret images from (a) and (b), and (a) and (c), respectively.

intensities smoothly changing between low and high. Images I (with $h(\mu) = 7.4/7.4/7.2$ and $h(\sigma) = 4.8/4.8/4.7$), L (with $h(\mu) = 7.8/7.8/7.7$ and $h(\sigma) = 5.3/5.3/5.3$), and Q (with $h(\mu) = 7.5/7.5/7.5$ and $h(\sigma) = 4.9/4.9/4.9$) are in this group. Third, the other images are in an interval of medium entropy values, and they are characterized by variations in some color ranges and with varying intensities, but not with very low or very high entropy values.

The normalized histograms of V_σ and V_μ for each color component from some special cases (*Image A*,*Image B*, and *Image O*) are presented in Figure 11, in Panels (a), (b) and (c), respectively. The special behavior in *Image B* incur in a low entropy for σ ($h(\sigma) = 3.1/3.1/3.1$) and high entropy for μ ($h(\mu) = 7.4/7.4/7.4$). The special behavior in *Image A* (with $h(\mu) = 7.6/7.6/6.9$ and $h(\sigma) = 3.7/3.7/4.1$) and *Image O* (with $h(\mu) = 6.6/7.3/6.4$ and $h_\sigma = 4.00/3.8/3.6$) takes place in V_μ dispersions of one color component, in one case with the blue component, and in the another case with the red component.

The summary statistics for RMSE values between $\hat{S}$ and S images generated with all T images (first dataset) are presented in Figure 12 (a). Two notably good results can be seen, which are related to *Image S* and *Image M*, with minimum values for RMSE of 3.59 and 4.73, and with median RMSE values of 7.45 and 8.43, respectively.

The median values related to MSSIM are also shown in Panel (b). In this case, *Image S* and *Image M* also present the two best values for MSSIM of 0.99 each one. We reinforce this statement with Figure 12 (c), where a representation of the relation between RMSE and MSSIM can be seen when using the whole set of images as a target. In Panel (d), only the *Image S* and *Image M* are considered as a target, thus highlighting the concentration towards better quality measures with them. Aiming to define the alternative criterion Λ mentioned in Eq. (12), and based in some of our previous analysis with the estimation errors, Figure 12 (e) and (f) presents the summary statistics for entropies $h(\mu)$ and $h(\sigma)$ in *Image S* and *Image M*. The criterion based in entropy values is empirically defined with: (1) $h(\sigma)$ values in the interval (4.3, 4.8); (2) $h(\mu)$ values in the interval (7.2, 7.6).

According to this, a new set of target images was collected, presented in Figure 6 of Section IV-A. Experiments for computing the quality measurements between original and recovered secret images were performed using this new set of target images. An average improvement can be seen in RMSE measurements about 18% with respect

to experiments performed with the first image set (called Mean PM), in Figure 12 (g) and (h) (NS stands for New Set in Mean NS). The MSSIM quality measure is not presented therein, as we had checked that its variation is very small and in many cases practically negligible.

In order to show a final example of the flexibility of the proposed method to choose the T^o_{opt} image, we selected the secret image in Figure 13 (a) since it is the one with the lowest performance, and the two target images in Panels (b) and (c), which give the best and the lowest performance, respectively. The resulting mosaic images are shown in Panels (d) and (f). Note that the recovered secret images, in Panels (e) and (g), look similar to the secret image, with some perceptible noise addition that increases in the second case.

E. SUBJECTIVE EVALUATION OF $\hat{S}$ in a Real Scenario

The visual quality of the images used in this work was evaluated over a DTT real scenario by an experiment with a Mean Opinion Score (MOS) analysis. The experiment took place in a laboratory setting, where a Transport Stream (TS) was transmitted by using a VHF/UHF modulator. The TS is a protocol for the transmission of audio, video, and data, as specified in the MPEG-2 standard, which helps in the multiplexing of audio, video and interactive applications by combining all data in a single stream of synchronized bits for its corresponding transmission. This signal was received by different types of receiver equipment (LCD, LED, and CRT) for the above-mentioned evaluation. Figure 14 shows the used scenario.

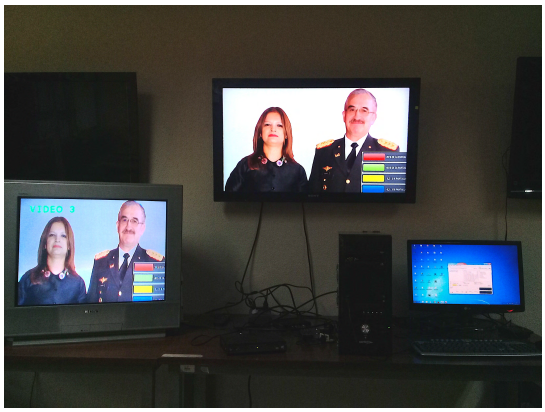

FIGURE 14. Scenario of transmission of a TS with interactive application.

The purpose of the interactive application developed for this analysis is to evaluate the quality of the received images when displayed in different sizes on the reception screens, i.e., when occupying 20% of the screen, 40% of the screen, and others. Figure 15 shows the interface of the application, where it can be selected the display options to evaluate the images, and the presentations of the images in different sizes, using the image carousel configuration for the interactive-application presentation. Images used to evaluate were included as M and $\hat{S}$ images obtained in the previous subsections.

FIGURE 15. Interactive application interface. (a) Selection menu for $\hat{S}$ image display size; (b) Display presentation occupying 20% of the screen; (c) Display presentation occupying 40% of the screen; (d) Display presentation occupying a ratio of 3.5:2 of the screen; (e) Display presentation occupying a ratio of 4.5:3 of the screen.

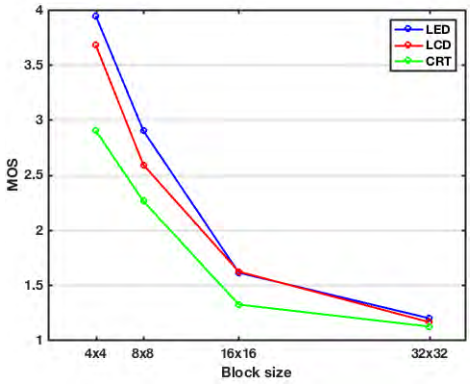

FIGURE 16. Subjective Evaluation of $\hat{S}$ in a Real Scenario using MOS method.

In Figure 16 we present the results obtained with the MOS analysis in the experiment. A total of 30 people participated, which were divided into groups of 10, so that each group could evaluate the pre-processed images in each of the different above-mentioned receivers. As expected, there is a relationship between the $\hat{S}$ quality and the block size. The screen used in reception that presents the best results is the LED technology. The image decoding at reception depends on the type of viewer, as the same interactive application with a single transmission can present different information.

V. DISCUSSION AND CONCLUSIONS

In this work, an algorithm to reduce the amount of bits required to retrieve a secret image embedded in a mosaic image, and to select the best target image, has been analyzed. On the one hand, we studied the empirical estimation and parametrization of the statistical distributions related

to image-block means and image-block standard deviations. On the other hand, we scrutinized the properties of the entropy of image-block means and of image-block standard deviations. The large amount of bits required to retrieve a secret image used in other applications is not practical for applications with limited resources, in [12] we can see a number of bits around 1600000 working with $u = 8$, which influences on the details similarity between the mosaic and target images. In the present work, we have developed this proposal in order to make efficient use of the resource available for interactive applications in the ISDB-Tb digital television system, since the bandwidth allocated for the transmission of multimedia information related to these applications is very restricted. We did not embed the required bits in the mosaic image because they can be transmitted externally at the same time. The method would be feasible and readily adaptable for gray scale images, though this direction was not scrutinized here.

The use of the Log-normal probability distribution to model the image-block standard deviations of the secret image, together with the estimation of the statistics of the blocks of the target image, allowed us to dramatically reduce (close to 3 to 1) the number of required bits while two images are transmitted in mosaic image format. Furthermore, a target image selection scheme has been developed to identify the most convenient one among a set of available target images. This has been carried out by analyzing the entropy of their image-block means and standard deviations in relation to RMSE and MSSIM, and looking for the specific characteristics of the images that help us in selecting the appropriate target image. This criterion has been defined for T image statistics entropy values, completely independent of the S image statistics, by the following steps: (1) $h(\sigma) \in (4.3, 4.8)$; (2) $h(\mu) \in (7.2, 7.6)$. The RMSE between the recovered and original secret images was improved in average by 18% with respect to the comparison of the results working with the first images set vs. the second set.

The MSSIM measure represent a kind of subjective similarity of the details, nevertheless, in digital television applications depending on the screen region assigned to image presentation we can expand the allowed error range. Future studies will be directed to apply further statistical simplifications to the position indices i_{σ_S} and i_{σ_T} and image-block means, among other low-complexity options. Other distributions could be scrutinized, though they could be bringing little significant advantage to the ones analyzed here. We currently continue to study the implications and significance of the subjective evaluation on the image visual quality in a laboratory broadcast scenario and in terms of Mean Opinion Score. Also within a DTT-research framework, we are currently using the NRCT and steganography techniques to embed images and data in a video stream. It would be very informative a larger-scale study on the impact of the method on the system global quality. Robustness to noise-caused critical errors in real-time applications should be checked with a different experimental design.

The proposed method allows us to reduce the number of bits required to recover secret image in reception, hence to improve the hiding capacity of mosaic images. It preserves the quality of recovered secret images, and it gives the possibility to determine the best target images available in DTT and in other multimedia application of interest.

REFERENCES

[1] *Official Site of Ginga Middleware*. Accessed: Apr. 20, 2018. [Online]. Available: http://www.ginga.org.br/en

[2] ABNT/CEE-085 TelevisÃčo Digital. *Digital Terrestrial Television—Data Coding and Transmission Specification for Digital Broadcasting Part 2: Ginga-NCL for Fixed and Mobile Receivers—XML Application Language for Application Coding*, document ABNT NBR 15606-2:2016 EN, Associacão Brasileira de Normas Técnicas, Río de Janeiro, Brasil, 2016.

[3] M. Gawlinski, *Interactive Television Production*. Oxford, U.K.: Focal Press, 2003.

[4] P. Kovesi, E.-J. Holden, and J. Wong, "Interactive multi-image blending for visualization and interpretation," *Comput. Geosci.*, vol. 72, pp. 147–155, Nov. 2014, doi: 110.1016/j.cageo.2014.07.010.

[5] D. Renza, L. D. M. Ballesteros, and R. Rincón, "Improved pixel hiding method for steganography of gray images within color images," *Ingciencia*, vol. 12, no. 23, pp. 145–162, 2016, doi: 10.17230/ingciencia.12.23.8.

[6] F. Li, K. Wu, X. Zhang, J. Yu, J. Lei, and M. Wen, "Robust batch steganography in social networks with non-uniform payload and data decomposition," *IEEE Access*, vol. 6, pp. 29912–29925, 2018, doi: 10.1109/ACCESS.2018.2841415.

[7] W. Hong, "Efficient data hiding based on block truncation coding using pixels pair matching technique," *Symmetry*, vol. 10, no. 2, pp. 36–53, 2018, doi: 10.3390/sym10020036.

[8] S. Zheng, D. Li, D. Hu, D. Ye, L. Wang, and J. Wang, "Lossless data hiding algorithm for encrypted images with high capacity," *Multimedia Tools Appl.*, vol. 75, no. 21, pp. 13765–13778, 2015, doi: 10.1007/s11042-015-2920-y.

[9] L. D. M. Ballesteros, D. Renza, and R. Rincon, "Gray-scale images within color images using similarity histogram-based selection and replacement algorithm," *J. Inf. Hiding Multimedia Signal Process.*, vol. 6, pp. 1156–1166, Jan. 2015.

[10] L. Laouamer and O. Tayan, "Performance evaluation of a document image watermarking approach with enhanced tamper localization and recovery," *IEEE Access*, vol. 6, pp. 26144–26166, 2018, doi: 10.1109/ACCESS.2018.2831599.

[11] I.-J. Lai and W.-H. Tsai, "Secret-fragment-visible mosaic image—A new computer art and its application to information hiding," *IEEE Trans. Inf. Forensics Secur.*, vol. 6, no. 3, pp. 936–945, Sep. 2011, doi: 10.1109/TIFS.2011.2135853.

[12] Y.-L. Li and W.-H. Tsai, "New image steganography via secret-fragment-visible mosaic images by nearly-reversible color transformation," *Advances in Visual Computing*, 2011, pp. 64–74, doi: 10.1007/978-3-642-24031-7_7.

[13] E. Reinhard, M. Adhikhmin, B. Gooch, and P. Shirley, "Color transfer between images," *IEEE Comput. Graph. Appl.*, vol. 21, no. 5, pp. 34–41, Sep./Oct. 2011, doi: 10.1109/38.946629.

[14] R. K. Lama, S.-J. Han, and G.-R. Kwon, "SVD based improved secret fragment visible mosaic image generation for information hiding," *Multimedia Tools Appl.*, vol. 73, no. 2, pp. 873–886, 2014, doi: 10.1007/s11042-013-1381-4.

[15] S. Kullback and R. A. Leibler, "On information and sufficiency," *Ann. Math. Statist.*, vol. 22, no. 1, pp. 79–86, 1951, doi: 10.1214/aoms/1177729694.

[16] F. Acosta, G. Olmedo, I. Mora, and J. L. Rojo-Álvarez, "An improved secure image transmission technique via mosaic images by nearly reversible color transformation," in *Proc. 14th Int. Joint Conf. e-Bus. Telecommun.*, 2017, pp. 87—92.

[17] N. Abramsom, *Information Theory and Coding*, R. Bracewell *et al.*, Ed. New York, NY, USA: McGraw-Hill, 1963, pp. 11–21.

[18] J. P. W. Pluim, J. B. A. Maintz, and M. A. Viergever, "Mutual-information-based registration of medical images: A survey," *IEEE Trans. Med. Imag.*, vol. 22, no. 8, pp. 986–1004, Aug. 2003, doi: 10.1109/TMI.2003.815867.

[19] J. Skilling and S. F. Gull, "Bayesian maximum entropy image reconstruction," in *Spatial Statistics and Imaging*, vol. 20, A. Possolo, Ed. Hayward, CA, USA: Institute of Mathematical Statistics, 1991, pp. 341–367.
[20] I. Lee, D.-C. Seo, and T.-S. Choi, "Entropy-based block processing for satellite image registration," *Entropy*, vol. 14, no. 12, pp. 2397–2407, 2012, doi: 10.3390/e14122397.
[21] B. Zhao, G. Qin, and P. Liu, "A robust image tampering detection method based on maximum entropy criteria," *Entropy*, vol. 17, no. 12, pp. 7948–7966, 2015, doi: 10.3390/e17127854.
[22] *PEXELS Best Free Stock Photos in One Place*. Accessed: Mar. 20, 2018. [Online]. Available: http://www.webcitation.org/6y3iUxhgu

FREDDY R. ACOSTA-BUENAÑO received the B.Eng. degree in electronic and telecommunications engineering from the Escuela Politécnica del Ejército ESPE (now Universidad de las Fuerzas Armadas ESPE), Quito, Ecuador, in 2002, and the M.Sc. degree in telecommunication networks for developing countries from Rey Juan Carlos University, Fuenlabrada, Spain, in 2012, where he is currently pursuing the Ph.D. degree with the Department of Signal Theory and Communications, Telematics and Computing. In 2004, he joined the Departamento de Eléctrica y Electrónica, Universidad de las Fuerzas Armadas ESPE, Sangolquí, Ecuador, where he has been an Associate Professor since 2008.

His current research interests include wireless communications, TCP, and digital terrestrial television broadcasting, telecommunications for assistance in the event of natural disasters, and stand-alone power supply systems for telecommunications systems.

INMACULADA MORA-JIMÉNEZ received the degree in telecommunication engineering from the Polytechnic University of Valencia, Valencia, Spain, in 1998, and the Ph.D. degree in telecommunication from the Carlos III University of Madrid, Madrid, Spain, in 2004. She is currently an Associate Professor with the Department of Signal Theory and Communications, Telematics and Computing, Rey Juan Carlos University, Madrid.

Her main research interests include statistical learning theory, and neural networks and their applications to image processing, bioengineering, and communications.

GONZALO OLMEDO received the B.Eng. degree in electronic and telecommunications engineering from the Escuela Politécnica del Ejército ESPE (now Universidad de las Fuerzas Armadas ESPE), Ecuador, in 1998, and the M.S. and Ph.D. degrees in electrical engineering from the Federal University of Campinas, UNICAMP, Brazil, in 2003 and 2008, respectively. Since 2005, he has been an Associate Professor with the Electrical Engineering Department, Universidad de las Fuerzas Armadas ESPE, where he has been the Head of the Department since 2011.

His current research interests include digital communications, wireless communications, OFDM, CDMA, channel codes, TCP, and digital terrestrial television broadcasting.

JOSÉ LUIS ROJO-ÁLVAREZ (SM'13) received the degree in telecommunication engineering from the University of Vigo, Spain, and the Ph.D. degree in telecommunication engineering from the Polytechnic University of Madrid, Spain, in 2000.

He was Senior Researcher in the Prometeo Program with the Universidad de las Fuerzas Armadas ESPE, from 2013 to 2015, Ecuador, and a Research Advisor with the Telecommunication Ministry. Since 2016, he has been a Full Professor with the Department of Signal Theory and Communications, Telematics and Computing, Rey Juan Carlos University, Madrid. He has published more than 110 papers in JCR journals and more than 150 international conference communications. He has participated in more than 60 projects (with public and private funding) and directed more than ten of them including several actions in National Plan for Research and Fundamental Science. In 2016, he received the Rey Juan Carlos University Prize for Talented Researcher.

His main current research interests include statistical learning theory, digital signal processing, and complex system modeling, with applications to cardiac signals and image processing.